

Improving the Modulation Bandwidth of GaN-Based Light-Emitting Diodes for High-Speed Visible Light Communication: Countermeasures and Challenges

Rongqiao Wan, Liancheng Wang,* Jinpeng Huang, Xiaoyan Yi, Hao-Chung Kuo, and Jinmin Li

Visible light communication (VLC) has attracted widespread attention for wireless communications. The popularity of GaN-based light-emitting diodes (LEDs) has also laid a solid foundation for the application of VLC. As the light source of VLC, LED's modulation bandwidth directly determines the speed of communication. Herein, reviewing progress on modulation bandwidth improvement schemes of GaN LEDs transmitter is reviewed, covering aspects from epitaxial to devices. Epitaxial approaches include c-polar facet epitaxial optimization, non/semipolar facet epitaxial growth, and chip scheme such as micro-LEDs, nano-LEDs, resonant cavity-LEDs (RC-LEDs), plasmon, and metacavity LEDs. In terms of white LEDs, approaches to tackle the slow Stokes transfer and long carrier life for conventional phosphors including new color-conversion materials (CCMs) and new energy transfer routes are reviewed. This review promotes the development of GaN-based LEDs as the transmitter for high-speed VLC.

1. Introduction

Visible light communication (VLC) has attracted great attention in recent years due to its advantages of high security, high speed, and no radio frequency (RF) interference. GaN-based light-emitting

diodes (LEDs) can be modulated at a much rapid rate that is imperceptible to the human eye, allowing them to convey a large capacity of information that satisfies the requirements of 5 G information society.^[1] More promisingly, solid-state lighting based white LEDs (WLEDs) have opened up new opportunities as each light bulb can act as a communication hotspot, integrating lighting and communication seamlessly and principally enabling communication at reduced cost and energy consumption.^[2]

Modulation bandwidth of LED is one of the most important factors that determine the communication speed and channel capacity. Resistance–capacitance (RC) time delay originated from the broad device area and quantum-confined Stark effect (QCSE) of the InGaN/GaN quantum wells (QWs) from intrinsic piezoelectric polarization field constrain the bandwidth of the LEDs for current phosphor converted chip, but also related to color conversion and fluorescent process. However, the fluorescent lifetime of the phosphor is long (> 50 ns), and there is also a Stokes shift process, making the optical bandwidth of traditional lighting-orientated phosphor-converted WLEDs be only a few MHz.

Much work has been done to increase the modulation bandwidth. Martin Dawson has provided an overview of the recent developments in VLC systems based on LEDs, covering aspects from sources to systems.^[3] In this article, we concentrate on reviewing research progress on modulation bandwidth improvement of GaN LEDs transmitter.

2. Basics Concept of LED Modulation for VLC


LED modulation bandwidth, generally -3 dB modulation bandwidth, is defined as the frequency at which the LED light output power (LOP) decreases at a low reference frequency to its half-value, as shown in **Figure 1a**. LED's modulation capacity is based on LOP versus current (P – I) characteristics, as shown in **Figure 1b**, which exhibits a quasilinear relation.

The modulation is achieved by varying the driving current. The light intensity varies correspondingly and is detected in the VLC system. The depth of the modulation, which is the ratio between the alternating current (AC) signal and direct current (DC) bias current, can be expressed as follows

R. Wan, L. Wang, J. Huang
State Key Laboratory of High Performance Complex Manufacturing
College of Mechanical and Electrical Engineering
Central South University
Changsha, Hunan 410083, China
E-mail: liancheng_wang@csu.edu.cn

R. Wan, X. Yi, J. Li
Semiconductor Lighting Technology Research and Development Center
Institute of Semiconductors
Chinese Academy of Sciences
Beijing 100083, China

H.-C. Kuo
Department of Photonics and Institute of Electro-Optical Engineering
National Chiao-Tung University
1001 Ta Hsueh Rd., Hsinchu 300, Taiwan

 The ORCID identification number(s) for the author(s) of this article can be found under <https://doi.org/10.1002/adpr.202100093>.

© 2021 The Authors. Advanced Photonics Research published by Wiley-VCH GmbH. This is an open access article under the terms of the Creative Commons Attribution License, which permits use, distribution and reproduction in any medium, provided the original work is properly cited.

DOI: 10.1002/adpr.202100093

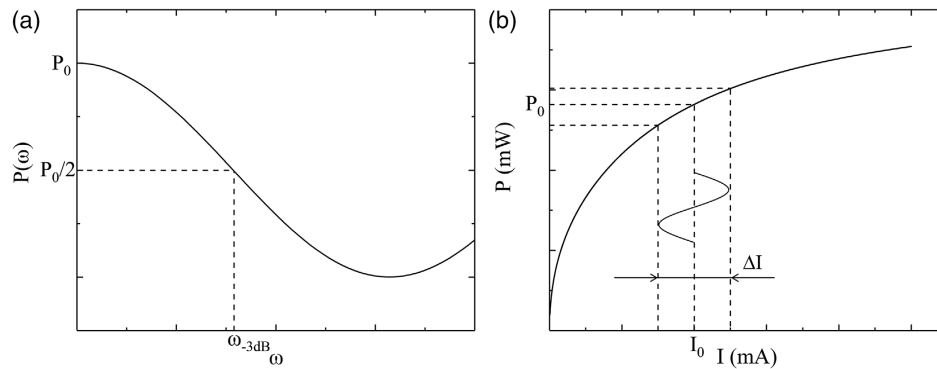


Figure 1. a) AC light power versus modulation frequency; b) power and current characteristics of LEDs.

$$m = \frac{\Delta I}{I_0} \quad (1)$$

where m is the modulation depth, I_0 is the bias current, and ΔI is the difference between the peak current and bias current.

3. Approaches for Improving LED Modulation Bandwidth

Modulation bandwidth of GaN LEDs is primarily determined by the velocity of carrier transport from the source to the active region and the recombination rate in the active region. The bandwidth of WLEDs is limited by the blue LED chip itself, Stokes transfer process, and the fluorescent process. Consequently, factors associated with carrier transport and recombination may affect the final modulation characteristics. **Figure 2** overviews the limiting factors of modulation bandwidth for LEDs and WLEDs.

Presently, the corresponding technical solution for enhancing the modulation characteristics of LEDs can be summarized as follows: 1) epitaxial innovation, including conventional c-polar epitaxial structure optimization and semi/nonpolar GaN epitaxial growth, to reduce QCSE effect; 2) smaller size LEDs to reduce the RC constant and increasing the carrier density and reduce QCSE effect; and 3) Purcell effect (plasmon, cavity) utilization to improve carrier recombination rate.

3.1. c-Polar LEDs Epitaxial Optimization Orientated for VLC

Approaches by adjusting and optimizing the epitaxial structure to manipulate the distribution of the carrier and increase the carrier's overlap and recombination rate have been reported.

J. K. Sheu from National Cheng Kung University decreased the thickness of GaN barrier layer from 17 to 5 nm, achieving -3 dB electrical-to-optical (E–O) bandwidth of 1 GHz with an active diameter of approximately $50\text{ }\mu\text{m}$.^[4] For conventional LEDs, due to the low velocity, i.e., nonuniform distribution of the injected holes, radiative recombination typically occurred at only one well closest to the p-side. Therefore, reducing the quantum barrier (QB) thickness should boost the transport of the injected holes and contribute to the radiative recombination at various wells. Although the total thickness of the active layer is

reduced from 97 to 37 nm, similar frequency response measurement results of the microwave reflective coefficients (S11) suggest that the RC-limited bandwidth is the same.

By further reducing both QWs/QBs to 1 nm/3 nm, Lai Wang from Tsinghua University demonstrated the cutoff frequency of 536 and 120 MHz at 2.5 kA cm^{-2} and 56 A cm^{-2} , respectively, for GaN devices with an area of $300 \times 300\text{ }\mu\text{m}^2$ grown on c-plane substrate.^[5] This is due to larger electron–hole wave function overlap in QWs and lower polarization effects for QW with thin barriers, leading to shorter differential carrier life and lower QCSE. However, because of the high nonradiative recombination, the LOP is significantly reduced. This mostly stems from the defects at the ultrathin QWs and QBs interface. Lixia Zhao from the Institute of Semiconductors varied the QW thicknesses to research the impact of QCSE and carrier localization effect. He reported that at low injection current density, QCSE dominates the recombination of the carrier and reduces the rate of radiative recombination. With an increase in the current density, the injected carrier screens the QCSE, thus improving the optical power and modulation bandwidth. When the polarization field is fully screened, the carrier localization effect begins to dominate. By reducing the QCSE and carrier localization effect, the LED with 5 nm QW and $60\text{ }\mu\text{m}$ area diameter achieves a high modulation bandwidth of 700 MHz at a low injection current density of 425 A cm^{-2} .^[6] Chao-Hsin Wu from National Taiwan University reported that compared with blue micro-LEDs with triple QWs, single quantum well (SQW)-based blue micro-LEDs have about 1.6 times higher modulation bandwidth, reaching to 752 MHz, and data transmission rates up to 1.5 Gb s^{-1} (two times) with $10 \times 10\text{ }\mu\text{m}^2$ area chip. This is attributed to more carriers being stored in the QW, resulting in a higher recombination rate and lower recombination lifetime.^[7] Guoyi Zhang from Peking University demonstrated the LEDs with superlattice-like strain relief layer (SRL), which can mitigate the nonlinearity of P – I and improve the signal-to-noise ratio (SNR).^[8] By using an external strain that nullifies the internal strain, Zhong Lin Wang group from Beijing Institute of Nanoenergy and Nanosystems reported that at a compressive strain of 0.14%, the highest speed of blue LED increased from 54 to 117 MHz.^[9]

As a weaker LOP leads to a poor SNR, it is important to increase the modulation bandwidth so that it is not detrimental to efficiency. In addition, a variety of factors including carrier

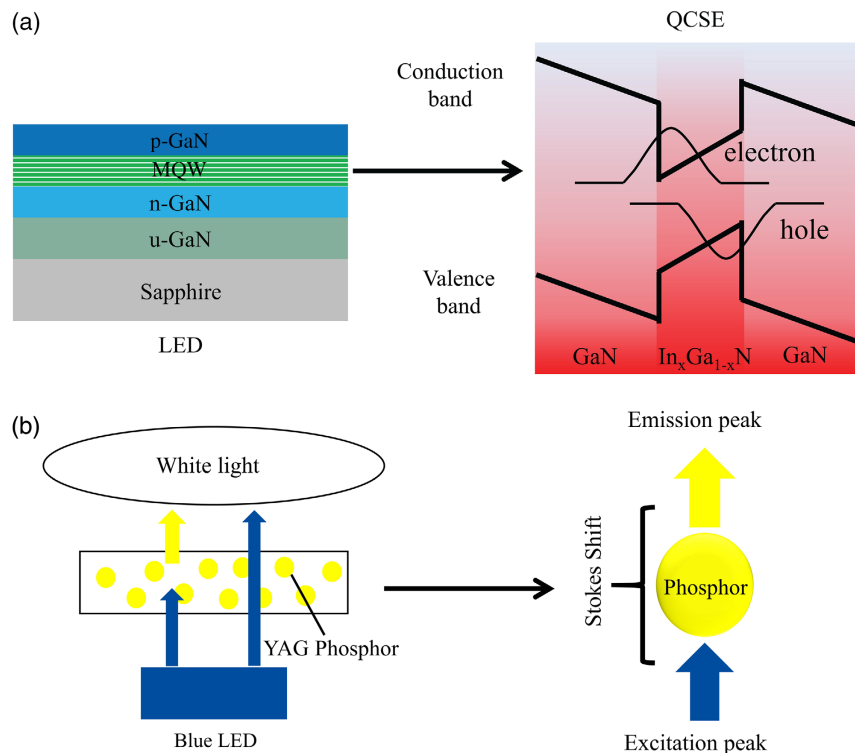


Figure 2. a) A typical epitaxial structure of the III-nitride LED and the schematic of QCSE; b) schematic of typical phosphor-based WLEDs and Stokes shift.

localization effect, defect, auger recombination, and QCSE can interfere and affect the modulation bandwidth. The efficiency at different current densities and the underlying physics mechanisms are still not properly understood. Particularly, note that LEDs are intentionally controlled at an exceptionally high current density to screen the polarization field to obtain a large bandwidth. It therefore requires intensive optimization of the VLC-oriented epitaxial structure of GaN LEDs, especially at low current density.

3.2. Semi/Nonpolar LEDs Epitaxial Growth

Previously recorded GaN-based LEDs were manufactured on the orientation of *c*-plane, which has been historically and extensively developed and optimized. However, it suffers from spontaneous and piezoelectric polarizations that stimulate internal electric fields within the active region and distort the energy band diagram, resulting in the well-known QCSE. Polarization fields can be screened by carriers at extremely high current density, but heat dissipation and efficiency drops may be a serious issue and thus make it not realistic.

Epitaxial growth in a nonpolar or semipolar direction should minimize and eliminate the effects of polarization, rendering larger wave function overlap and shorter carrier lifetime, providing a path to greater modulation bandwidths than *c*-plane LEDs, particularly at low current densities. **Figure 3** shows the difference in energy band structure when QWs are grown on *c*-plane and *a/m*-plane, respectively.

For semipolar LEDs, the internal fields are reduced depending on the angle of inclination with respect to the *c*-axis. Epitaxial growth on (11–22) shows a polarization field of almost zero. In addition, the incorporated indium atoms have lower repulsive interactions than those on nonpolar or polar surfaces, indicating that semipolar (11–22) GaN surfaces can accommodate more indium atoms than nonpolar or polar surfaces, making them more suitable for achieving longer wavelength emitters.^[10]

According to the traditional ABC model, carrier recombination rate equation $R(n)$ can be expressed as

$$R(n) = An + Bn^2 + Cn^3 \quad (2)$$

where A , B , and C are the coefficients of Shockley–Read–Hall, radiation, and auger, respectively; n is the carrier concentration when a small current is injected. For small-sized LEDs, the main factor limiting the highest modulation frequency is the carrier life rather than capacitance.

The –3 dB modulation bandwidth can be simply expressed as

$$f_{-3dB} = \frac{\sqrt{3}}{2\pi\tau} \quad (3)$$

where τ is the carrier lifetime, which is closely related to the carrier density, n , injected into the active region. Thus, τ can be expressed as follows^[11]

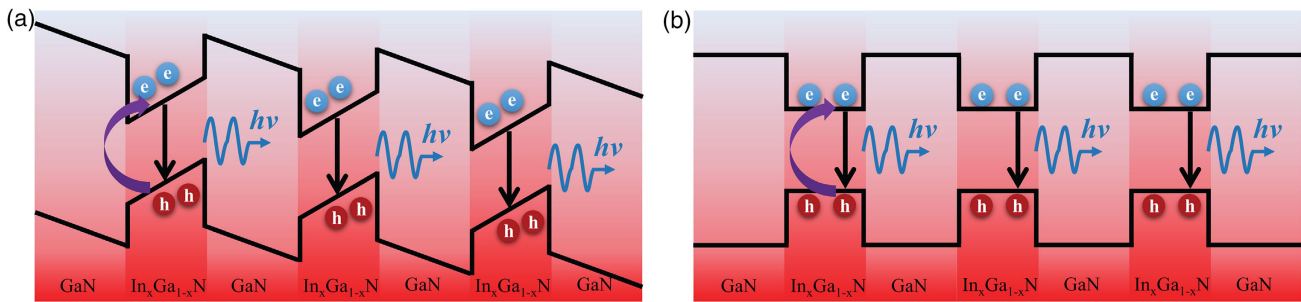


Figure 3. Energy band structure when QWs are grown on a) c-plane and b) a/m-plane.

$$\tau = \frac{n}{R(n)} = \frac{1}{A + Bn + Cn^2} \quad (4)$$

Therefore, combining Equation (3) and (4), we can obtain

$$f_{-3dB} = \frac{\sqrt{3}}{2\pi} (A + Bn + Cn^2) \quad (5)$$

From the above equations, it is not difficult to see that the -3 dB bandwidth of LED is closely linked to recombination process and carrier concentration. Coefficients A , B , and C are mainly determined by the material defect density, overlap probability of electron-hole wave functions, and high current injection, respectively. Obviously, any increase in the coefficients A , B , and C is conducive to the increase in bandwidth. However, the increase in the coefficients A and C will cause more carriers to recombine through the nonradiative channels, which will affect the luminous efficiency. Only by increasing coefficient B can improve bandwidth and luminous efficiency simultaneously. Therefore, compared with polar LEDs, semi/nonpolar LEDs have a higher probability of electron-hole wave function overlap, resulting in higher bandwidth and luminous efficiency.

P. J. Parbrook from Tyndall National Institute, University College Cork reported that $30 \times 30 \mu\text{m}^2$ LEDs with 8 nm-thick quantum well grown on semipolar (11–22) GaN templates have a modulation bandwidth of over 800 MHz and data transmission rate of 1.5 Gb s^{-1} under nonreturn-to-zero on-off keying modulation scheme at 385 A cm^{-2} .^[12] Daniel Feezell from the University of New Mexico reported a nonpolar m-plane InGaN/GaN microscale LED with an electrical -3 dB modulation bandwidth of 1.5 GHz and a carrier differential lifetime (DLT) of 200 ps at 1 kA cm^{-2} .^[13] Hao-Chung Kuo from National Chiao Tung University demonstrated a green semipolar (20–21) InGaN/GaN micro-LED with the highest -3 dB bandwidth of 756 MHz and a data transmission rate of 1.5 Gb s^{-1} at 2.0 kA cm^{-2} .^[14] And they also demonstrated single semipolar QW (3 nm) blue LED with the bandwidth to be 428, 858 MHz, and 1.057 GHz at 500 A cm^{-2} , 1.5, and 2.5 kA cm^{-2} , respectively. The anisotropic growth rate for different directions results in unsmoothed surface with stripes or grooves, which poses as a great challenge for semi/nonpolar MQWs growth. For example, for semipolar (11–22), growth proceeds along [1] c-direction and [11–20] or a-direction, and negligible growth rate at [1100] or m-direction. The c-direction shows a faster growth rate than a-direction, resulting in the formation of inclined stripes on

the surface. However, the crystal quality of semipolar or nonpolar GaN directly grown on sapphire is worse than c-plane GaN counterpart. As a result, considerable effort is required to improve the crystal quality, and optimize the epitaxial structure and chip fabrication process.

3.3. Micro-LEDs

Micro-LEDs refer to LEDs with active area of less than $100 \mu\text{m}$ based on traditional epitaxial structure. With lower capacitance, lower thermal effect, and good current diffusion, micro-LEDs can be powered at a substantially higher current density than broad-area LEDs.^[15,16]

In 2010, Martin Dawson group reported micro-LED's E-O modulation bandwidth of 245 MHz with $72 \mu\text{m}$ diameter and 450 nm peak emission wavelength, manufactured with standard epitaxial structure and chip process.^[17] Further experiments revealed that smaller micro-LEDs exhibit larger maximum modulation bandwidth because it can sustain higher saturated current density, yet each micro-LED had a similar bandwidth for the given injected current density. This indicates that the RC time constant is not the limited factor and QCSE should be similar for micro-LEDs with various areas.

This observation is best explained by the determination of DLT of QW carriers. When the current density increases with reduced DLT, it results in a larger modulation bandwidth. To further enhance the modulation bandwidth and linearity of single pixel micro-LEDs, chip structure design and fabrication process optimization were adopted. Martin D. Dawson reported on new micro-LED designs with a bandwidth of more than 800 MHz. The design adopts Pd to improve the metallization of p-contact. In addition, deep etching from the mesa to the substrate reduces the capacitance.^[18] Gang Wang from Sun Yat-Sen University demonstrated micro-LEDs using an aluminum-doped zinc oxide transparent current diffusion layer of 300 nm; the micro-LEDs with a $150 \mu\text{m}$ mesa diameter have a maximum LOP of 42 mW, a modulation bandwidth of 600 MHz, and a free-space data transmission rate of 3 Gb s^{-1} .^[19]

However, the smaller the size of the device, the smaller is the active area, and the impact of sidewall defects on the device gradually becomes larger. According to Equation (4), it can be seen that the increase in coefficient A can improve the modulation bandwidth, but a certain optical power is sacrificed, resulting in poor SNR restrict large modulation of the signal. By operating micro-LEDs in an array fashion, a significantly improved optical

power and high simultaneous transmission rates can be guaranteed. The influence of pixel size on the array, array structure, and layout configuration on the performance has been investigated.^[20] Furthermore, there have been reports on the potential of microLED arrays for single-chip multichannel data transmission, VLC, and display dual functions by integrating them with complementary metal–oxide–semiconductor (CMOS) drivers^[21,22] and AlGaIn/GaN high electron mobility transistor (HEMTs)^[23].

For micro-LED, its geometric capacitance is much smaller than that of broad-area LED, so capacitance is not the main factor limiting the maximum bandwidth. According to the thermal power equation $P = I^2 R$, when the same current density is applied to micro-LEDs and LEDs, the current for micro-LEDs will decrease by n -fold, which is the area ratio between broad-area LEDs and micro-LEDs. Even though the resistance increases by n -fold, the final power consumption is reduced by n -fold. This is the main reason why micro-LEDs are capable of maintaining high current density and thus achieving high bandwidth modulation. Note that for micro-LEDs, QCSE is almost similar compared with broad-area LEDs. However, the high current density leads to a substantial drop in efficiency, which makes it impossible to ignore the long-term reliability issue even if heat generation is reduced compared with the broad-area LED. Martin Dawson also reported a 400 nm emitted violet micro-LED with an E–O bandwidth of up to 655 MHz and a data transmission rate of 11.95 Gb s^{-1} .^[24] Although QCSE decreases compared with the longer wavelength micro-LEDs, internal quantum efficiency (IQE) drops sharply at shorter violet emission wavelengths.

3.4. Nano-LEDs

By further reducing the size from the micrometer scale to the nanometer scale, strain can be released and simultaneously maintained to work at a higher current density as micro-LEDs, thus achieving a higher bandwidth modulation. Jian-Jang Huang from National Taiwan University reported that a photonic crystal (PhC) LED with a smaller $20 \mu\text{m} \times 20 \mu\text{m}$ ($120 \mu\text{m} \times 120 \mu\text{m}$) mesa size demonstrates a 347 MHz (112 MHz) small-signal E–O – 3 dB bandwidth and recommended that PhC-LEDs have a larger period and air-hole portion.^[25] He also reported that PhC-LEDs may not perform well at low data rates due to their relatively lower SNR, but they exceed conventional LED structures, especially at higher data rates.^[26] The bandwidth improvement of PhC-LEDs is primarily attributed to two factors. First, by specifically designing the PhC to match the emission band diagram, it makes it possible to achieve a faster photon decline rate, higher photonic modal extraction, and shorter radiative recombination lifetime. Second, the nanoholes of PhC-LED contribute to alleviate strains and QCSE. Daniel Feezell from University of New Mexico reported electrically injected GaN/InGaIn core–shell nanowire LEDs with –3 dB modulation bandwidth of 1.2 GHz at 1 kA cm^{-2} .^[27] A new method of colloidal photolithography based on Talbot effect for the manufacturing of nano-LEDs, including nanohole, nanorod, nanoring, and anti-nanoring LEDs, with a lifetime of 12, 6, 4, and 8 ns in the typical time-resolved photoluminescence (TRPL) test compared with 15 ns of broad-area LEDs, was reported.^[28] The advantages of nano-LEDs for VLC include continued

operation at higher current density, relief of strains and mitigation of QCSE, higher light extraction efficiency, and a PhC cavity design to boost optical power and reduce radiative recombination time.

Disadvantages of nano-LEDs for VLC include more complicated fabrication process, and need special lithography system and processing, for example, electron beam lithography; most nano-LEDs are fabricated by etching deeply into the n-GaN region, defects generated during the dry etching process, and seriously degrade the electrical property. Daniel Feezell stated that the differential recombination lifetime ($\approx 330 \text{ ps}$) is much longer than the RC time constant ($\approx 30 \text{ ps}$) measured at 1 kA cm^{-2} , which confirmed that the effect of RC parasitic delay on modulation speed can be ignored. The carrier injection, QW thickness, and indium composition are not uniform across the nanowire, resulting in anomalies and unreliable behaviors in nano-LEDs.

3.5. Resonant Cavity-LEDs

According to Purcell effect and Fermi golden rule, engineered photonic structures such as resonant microcavity can regulate the intensity and distribution of electromagnetic fields in space. The luminescence properties include: increase in the optical mode density at resonance wavelength; improvement in the spontaneous emission rate, thus the modulation bandwidth; screening modes which satisfy the condition of constructive interference and reduction in the luminous spectrum width; manipulation of the distribution of internal light power angle; confinement of photons into the escape cone angle; and improvement in the light extraction efficiency. These properties make resonant cavity-LEDs (RC-LEDs) particularly attractive for fiber-based VLC, where the enhanced directionality and spectral purity, respectively, enhance coupling to fibers and reduce chromatic dispersion.

E. F. Schubert reported the highly efficient and directional GaAs-based Fabry–Perot microcavity LED.^[29] However, the epitaxial growth of appropriate distributed bragg reflector (DBRs) in the AlInGaIn alloy system is challenging. The most apparent approach to growing III-nitride DBRs is to vary the AlN fraction in AlGaIn layers. Shaw et al. modeled RC-LEDs with such DBRs explicitly for VLC applications with plastic optical fiber (POF).^[30] However, only a small refractive index differences between the adjacent DBR layers can be achieved in the AlGaIn system, and increasing the number of layers to increase reflectivity will lead to serious problems of strain management. AlInN can be lattice matched to GaN itself at an InN fraction of $\approx 18\%$, and nominally strain-free DBRs can also be grown with various combinations of AlGaIn and AlInN layers. The disadvantages of working with AlInN in metal organic chemical vapor deposition (MOCVD) include slow growth rate and the repeated temperature ramps required during DBR growth. Data rate at 200 Mb s^{-1} over 100 m of POF was reported by Akhteret using a RC-LED with a peak emission wavelength of 509 nm,^[31] and Tsai et al demonstrated 100 Mb s^{-1} transmission over 100 cm of free space using a blue-emitting RC-LED.^[32] Hao-Chung Kuo from Taiwan National Chiao-Tung University in situ grown AlN/GaN DBR by MOCVD to form one side of the GaN-based photoelectric

device Fabry–Perot cavity.^[33] Professor Bao-Ping Zhang group from Xiamen University fabricated vertical-structured Fabry–Perot cavity on Si substrate by metal bonding technique;^[34] Yongjin Wang group from Nanjing university of Posts and Telecommunications and Professor Amano from Japan Nagoya University Hiroshi deposit $\text{TiO}_2/\text{SiO}_2$ DBR on top and bottom for RC micro-LEDs.^[35]

The spontaneous emission rate enhancement depends on the emission wavelength, cavity parameters, and dipole orientation. Change in lifetime is limited for practical cavities, as several experiments have reported. The largest decrease in recombination lifetime is achieved with a high-Q cavity, yet it corresponds to a small cavity bandwidth, which means that only emission at limited wavelengths within the LEDs spectrum could be “accelerated.” The radiative recombination speed boost after averaging the recombination lifetime of an electron–hole pair over all available energy levels of the electrons and holes in the active region of LEDs is constrained.

3.6. Plasmonic LEDs and Metacavity LEDs

Plasmonic nanolasers can support ultrafast dynamics and ultra-small mode volumes. Concentrate light by plasmon leads to electrical field enhancement and can be used to manipulate the light–matter interactions and accelerate LEDs. Basically there are two types of metal plasmon: surface propagating plasmons (SPPs) and localized surface plasmon (LSP). SPPs show nonresonant characteristics and generation of SPPs should satisfy the k-vector match requirement, while LSP exhibits resonant characteristics and no k-vector matching requirements are needed. In addition, the low mode volume means the effective coupling distance between the emitter and the plasmon is quite short on the order of several tens of nanometers. The electron–hole recombination mechanism of plasmonic LED is shown in **Figure 4a**.

Okamoto et al. reported the resonant coupling between the blue-emitting InGaN/GaN QWs without a p-GaN layer and bulk-like silver. He concluded that the roughness of the metal layer contributes to the k-vector matching.^[36] As the p-GaN layer for GaN LEDs is between 100 and 200 nm, some methods have been conceived and reported to locate the metal particles near the QWs. Processed into nanocolumns down to the QW active region, where discrete silver nanoparticles (NPs) are embedded and then replanarized by spin-on glass, Zhu et al. reported LEDs with E–O bandwidths of ≈ 30 MHz,^[37] which is approximately twice that of control devices without the silver NPs. Yang et al. developed an inverted hexagonal pyramid LED, which

grows naturally in specific MOCVD growth regimes and is coated with silver metal layer. It showed a bandwidth of 200 MHz, with 100 μm diameter at DC 10 V, whereas the device without a silver layer had a bandwidth of 115 MHz.^[38] Zhaowei Liu from the University of California, San Diego, reported a nanostructured plasmonic LED (PLED) consisting of a nanohole grating coated with a thin silver layer.^[39] It was suggested that the PLED can theoretically realize a -3 dB bandwidth of about 8.5 GHz through the experimentally measured carrier lifetimes. Xiang Zhang from UC Berkeley exhibited the coupling between three-dimensionally nanofocused plasmonic modes and single quantum dots (QDs) InGaN without any positioning.^[40] By depositing a thin silver layer on a site-controlled pyramid QD wafer, 3D plasmonic nanofocusing was geometrically achieved at the pyramid apex on each QD. For all processed QDs emitting over ≈ 150 meV spectral range, the spontaneous emission rate of the QD was enhanced by up to 22 ± 16 .

Although the mode volume of plasmon is small, the Q-factor is large due to inherent metal joule loss. However, they suffer from high radiative losses due to the significant momentum mismatch between their nanolocalized lasing fields and free-space light, which could be practically beneficial for wide spectrum enhancement.

Full realization of the potential of plasmonic effects in high-speed III-nitride LEDs poses numerous challenges, including additional continuous metal layers for current dissemination and external contacting. Some more complex metal plasmon structures can be envisioned to counter the metal Joule loss in plasmon. Teri W. Odom from Northwestern University investigated 2D plasmonic Au or Ag NPs arrays surrounded by a gain medium, in the deep subwavelength vicinity of the individual NPs by stimulated energy transfer from the gain to the band-edge lattice plasmons.^[41] Hyperbolic metamaterial (HMM) with multiple metal–dielectric interfaces using nanorod arrays or multiple layers were presented for which the principal components of the uniaxial permittivity tensor had opposite sign.^[42] This resulted in an anomalous dispersion with an indefinite hyperbolic isofrequency contour (IFC). The hyperbolic dispersion led to a high state photonic density (PDOS), which by the Purcell effect enhanced the spontaneous emission rate of light emitters. It supports the propagation of a broad range of wavevectors, confirming that plasmonic modes were confined at a deep-subwavelength scale in all three dimensions. A nanometer-scale hyperbolic metacavity array, where all excited plasmon oscillations within the metacavity can couple in one lasing mode and spontaneous emission rate is enhanced by 30 folds, was specifically designed.

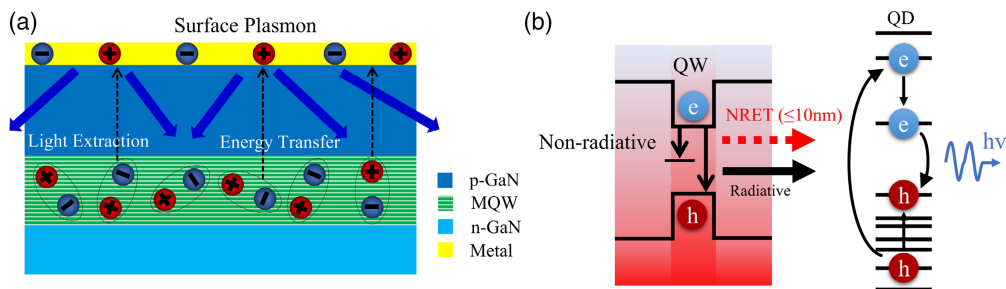


Figure 4. a) The electron–hole recombination mechanism of plasmonic LED; b) the physical schematic diagram of a NRET process.

3.7. WLEDs

For WLEDs, the modulation bandwidth is determined by LED chip and color conversion material (CCM), which is further limited by the slow phosphor and Stokes transfer process. Lifetime of conventional YAG phosphorus is ≈ 70 ns. To overcome this drawback, some new CCMs are constantly being investigated. For example, compared with phosphors, QDs not only have high quantum yield, but also have a shorter fluorescence lifetime.^[43,44] The disadvantage of QDs is that their FWHM is too narrow, which can easily cause spectral vacancy, and the stability needs to be further improved.^[45,46] **Table 1** outlines the typical lifetime of the new CCMs used and the corresponding modulation bandwidth. For example, Lixia Zhao from Institute of Semiconductors, CAS reported blue LED chip with GHz bandwidth combined with CdSe/ZnS QDs to achieving 637.6 MHz QD-converted WLED and 675 Mb s⁻¹ real-time nonreturn-to-zero on-off-keying signal without optical filters at 20 kA cm⁻², with a low bit error rate of 4.35×10^{-8} ; coordinate is almost close to the edge of white light area with the correlated color temperature (CCT) $\approx 10\,000$ K.^[47] It can be seen that the lifetime of CCMs is in the ns level, but for the GHz-level LED chip, its carrier life is less than 1 ns, and the light emission of CCM needs to undergo Stokes shift, so the high-speed communication application of fluorescent WLED still has great challenges. Martin D. Dawson and Harald Haas, using a blue μ LED combined with conjugate polymer and an adaptive direct current biased optical-orthogonal frequency division multiplexing (DCO-OFDM) technique, achieved a white light communication link of 1.68 Gb s⁻¹ at a distance of 3 cm, but an illumination level far lower (240 lx) than that of a commercial WLED.^[48] Furthermore, due to its small size, the nonradiative energy transfer (NRET) effect can be used to activate new channels for energy transfer and wavelength conversion, as shown in Figure 4b. For example, by combining nanohole LEDs and QDs, Liu demonstrated a hybrid III-nitride/nanocrystal WLED with a high NRET efficiency (up to 80%), color rendering index (CRI) is 82, and CCT ranges from 2629 to 6636 K.^[49]

Although many new CCMs (such as QDs) are constantly being recommended to replace phosphors, these materials have poor stability and still have a longer fluorescence duration than the life of the carriers recombination of the LED chips. This means that CCM always limits the bandwidth of the WLEDs. Therefore, the application of single chip WLED in VLC is proposed.^[50] Therefore, phosphor-free single chip WLEDs were fabricated with tunable CCT (from 1600 to 6000 K), broadband spectrum (from 400 to 750 nm), moderate CRI (≈ 75), and significantly improved modulation bandwidth (maximum of 150 MHz) at

low injection current density of 72 A cm⁻² by using self-assembled InGaN QDs structure.^[51] The broadband spectrum is ascribed to the carriers captured by various localized states of InGaN QDs. In addition, compared with the conventional InGaN/GaN QWs structures, the QDs structure has an alleviative QCSE, which is beneficial to improve the recombination rate. Thus, the single chip WLED can provide a high bandwidth at a relatively low injection current density.

Figure 5 shows the modulation bandwidth of LED chip at a specific current density. **Table 2** overviews and summarizes the limiting factors, countermeasures, challenges, and prospects to increase the modulation bandwidth of LED and WLED. For epitaxial materials, due to the strong polarization effect of nitrides, the QCSE of QWs is a major factor limiting the carrier recombination rate, which can be reduced by growing non/semi-polar epitaxy or optimizing epitaxial structure. For the LED chip, the device structure design can also improve the carrier recombination rate. For example, higher current injection density can be achieved by reducing the size of LED chip, microstructure can be designed to release the stress in QWs, or optical microcavity can be designed to improve spontaneous emission. For WLED, the Stokes shift and longer fluorescence lifetime of CCMs are the main factors limiting the bandwidth. Therefore, CCMs with short fluorescence lifetime are constantly studied, and optical design can also be used to improve the luminescence rate of CCM, such as plasmon. Furthermore, the technology route of phosphor-free single chip WLEDs may be an effective way to get rid of the bandwidth limitation of CCMs.

4. Influence of Modulation Depth on the Modulation Width

Micro-LEDs are usually driven at very high current densities of \approx kA cm⁻² order, which is much higher than the current operating density of broad-area LEDs of less than the order of 10² A cm⁻², to achieve high modulation bandwidth of the order of 10² MHz. Very high current densities driving the micro-LEDs can result in significantly higher carrier recombination rates, strongly oblique band diagrams, and a large electric field in the p-i-n region, in sharp contrast to broad-area LEDs. The modulation width influences the electrical field in the active region and rise-fall time of the device electroluminescence, thus the modulation width. Pengfei Tian from Fudan University reported that as the input electrical modulation power increases, the modulation bandwidth of the micro-LED slowly drops from 180 MHz

Table 1. Comparison of characteristics of GaN-based WLED.

λ [nm]	Current density	Conversion material	Lifetime	Bandwidth [MHz]	Reference
470	20 kA cm ⁻²	CdSe/ZnS QDs	17.24 ns	637.6	[47]
445	1.1 kA cm ⁻²	Perovskite QDs	43.74 ns	85	[54]
460	–	CdSe/ZnS QDs	11.2 ns	9.8	[55]
450	–	AgInS ₂ /ZnS QDs	77 ns (green), 193 ns (red)	5.4	[56]
395	–	dye@metal-organic framework fluorophore	1.8 ns (blue), 5.4 ns (yellow)	3.6	[57]
–	–	CdSe/ZnS QDs	29.3 4 ns (green), 26.31 ns (red)	2.6	[58]

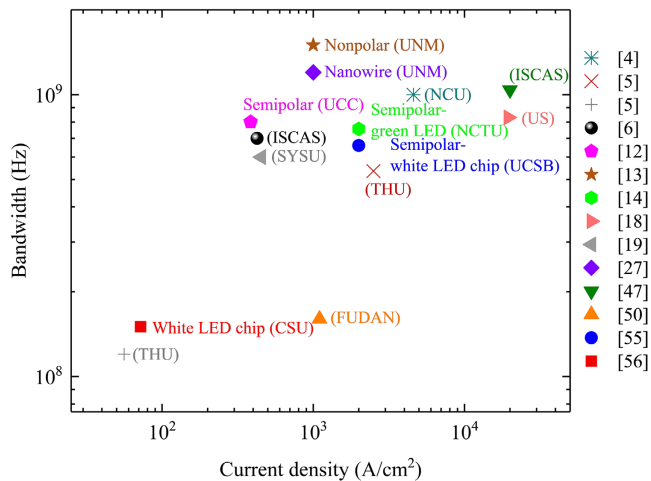


Figure 5. The modulation bandwidth of the LED chip at a specific current density.

at -15 dBm to 173 MHz at 2.5 dBm and then rapidly drops to 160 MHz at 10 dBm.^[52] This was further explained based on band diagram at various voltage statuses: from 0 to 3.1 V, the energy of conduction band on the n-side increases. While at 3.1 V, the energies of the conduction band on n-side and p-side are almost similar. From 4.1 to 5.1 V, an increase in the conduction band on the n-side caused conduction band to tilt strong from the n-side to the p-side.

The induced wide electric field can sweep the electrons from the n-side to the p-side, resulting in a reduced time constant at a higher voltage. Both the carrier recombination and the carrier sweep-out effects lead to a faster rise time and slower fall time, and these effects are more substantial when the modulation depth is greater. Bandwidth is determined by the sum of the rise and fall times.

5. Influence of LOP–Current Density (P – J) Linearity on the Modulation Width

Gang Wang from Sun Yat-Sen University reported a GaN LED structure with a mesa diameter of 150 nm, a maximum optical power of 42 mW, and a transparent current diffusion layer of 300 nm aluminum-doped zinc oxide, which showed an improvement in the linear relationship between power and voltage and exhibited a 3 Gb s $^{-1}$ free-space data transmission rate.^[19] Guoyi Zhang reported that the linear relationship of P – I was improved by using SRL.^[8]

An improved power versus current density (P – J) linearity is suitable for high-data rate VLC. The nonlinearity characteristics of LEDs generate issues such as amplitude distortion and signal clipping under the spectrally efficient analog modulation schemes. Circuit components for equalization need to be attuned to individual LEDs, which increase the complexity of VLC systems, especially for large-scale LED-based lighting systems. Moreover, if the required modulation bandwidth is very broad, such as over 500 MHz, then general distortion compensation circuit techniques such as predistortion and feed-forward are not necessarily effective. It is also difficult to use in the wide bias and temperature regions. Such broadband devices need distortion reduction at chip level.

The P – I nonlinearity originates from the GaN LED efficiency drop, which has been extensively studied. The underlying mechanism includes polarization field, Auger recombination, current crowding, and electron leakage. Countermeasures to prevent a drop in efficiency should help mitigate the of P – I nonlinearity.

The increase in carrier concentration in the active region leads to decreased carrier's DLT. According to Equation (4), when the coefficient A is large, more carriers are captured by the defect, resulting in low optical power, as shown in **Figure 6a**. However, defect energy levels provide more recombination channels for carriers to reduce the recombination lifetime of carriers,

Table 2. Limiting factors, countermeasures, challenges, and prospects to increase the modulation bandwidth of LED and WLED.

	Limiting factors	Countermeasures	Challenges and prospects
Epitaxial	QCSE	Non/semipolar epitaxial	Low crystal quality, not optimized epitaxial, and chip processing
		C-polar optimization (QW, QB thickness, QW number, etc.)	Efficiency and modulation bandwidth balance Carrier localization, defect, and Auger recombination
LED chip	QCSE	Micro-LEDs	Current density too high, efficiency droop and low power, heat dissipation, QCSE
	Current saturate and heat dissipation	Nano-LEDs	Complicate fabrication, specially lithography, defects generated during dry etching; large series resistance
		RC-LEDs	Enhanced directionality and spectral purity for PFC VLC Resonant enhancement not effective for wireless VLC
		Plasmon, metacavity LEDs	Special chip structure, difficult electrical contact, optical quench
WLEDs	QCSE	Micro-LEDs+ new CCM	Current density too high, efficiency droop and low power, heat dissipation, QCSE; not optimized lighting performance
	Slow Stokes transfer	Micro-LEDs array+ new CCM	Current density too high, efficiency droop, heat dissipation, QCSE; not optimized lighting performance
	Long carrier life time phosphor	Plasmon WLEDs	Special chip structure; not optimized lighting performance
		NRET WLEDs	Near field requirement and restriction
		InGaN QD without phosphor	Not optimized epitaxial and lighting performance

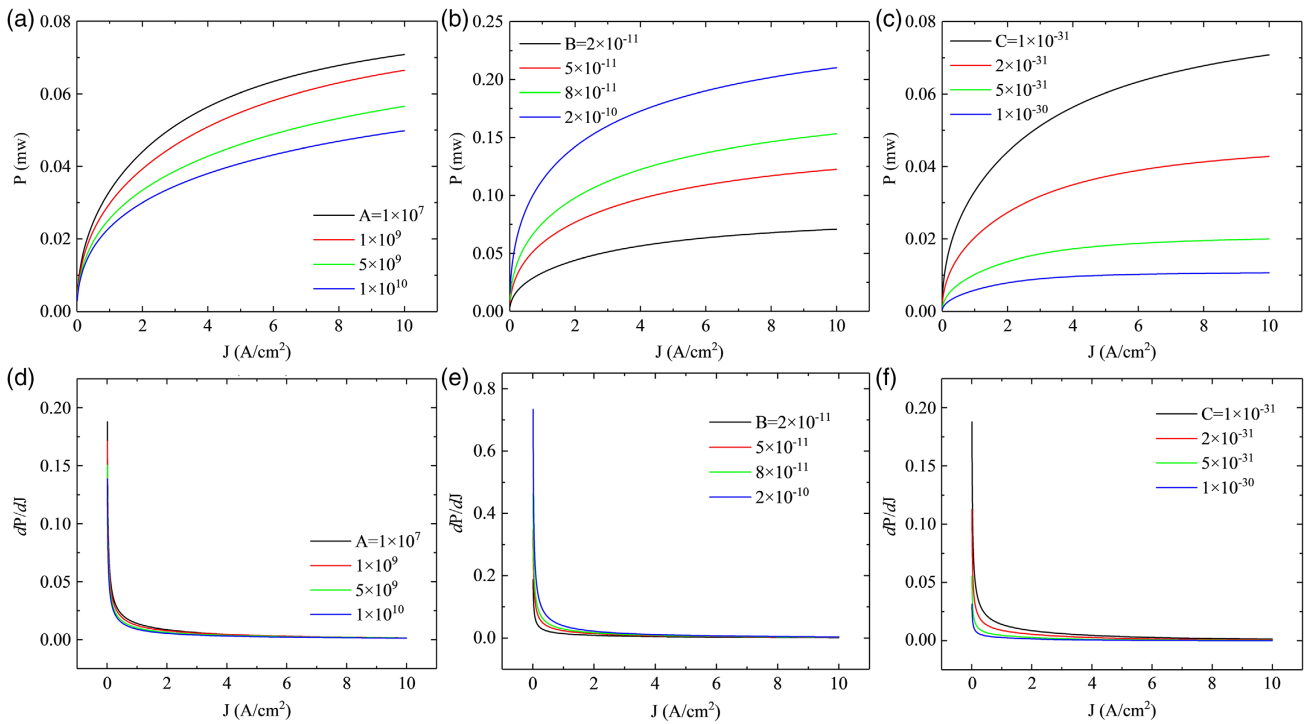


Figure 6. P - J curves under various a) A , b) B , and c) C and current density; b) dP/dJ curves under various d) A , e) B , and f) C and current density.

leading to an increase in bandwidth, at a greater sacrifice on optical power. An increase in coefficient B increases the optical power, as shown in Figure 6b. The bandwidth and signal strength can be improved simultaneously, which is ideal for VLC applications. At large current, the coefficient C has the greatest impact on the carrier recombination rate. Comparing Figure 6a-c, it is obvious that the change in the coefficient C has a more sensitive effect on the optical power than the coefficients A and B .

When a small current is injected, the recombination of carriers at the defects quickly reaches saturation, and more carriers participate in the radiative recombination of the quantum well region, resulting in a faster increase in optical power in the initial stage. The larger the coefficient A , the more defects are in the material, and the more carriers will be trapped by the defect energy level, so the rate of increase in the optical power will be slower, as shown in Figure 6d-f. As the injected current increases, when the carriers do not fill the quantum well, the optical power exhibits a quasilinear increase, but the rate of increase gradually decreases as the carriers in the quantum well gradually saturate. When the coefficient B is larger, it implies that the electron-hole wave function overlap probability is larger in the active region, resulting in more carriers undergoing radiation recombination. Therefore, both the optical power and the growth rate of optical power will be significantly improved. Under large current injection, the carriers in the quantum well region have reached saturation, and the excess carriers will consume the generated energy in the form of phonons through Auger recombination. Therefore, it can be clearly seen that the optical power gradually becomes smooth and grows slowly at large current.

An increase in the coefficient C implies a higher proportion of nonradiative recombination of the carriers, which not only reduces the optical power, but also ensures that maximum optical power enters the smooth region earlier.

For indoor lighting, underwater communications,^[53] and so on, we hope that the device has higher optical power and linearity, but for some short distance transmission, such as video stream, higher modulation bandwidth is required than optical power. So, we should find a balance point for the application of VLC and increase the bandwidth as much as possible under the premise of satisfying the signal strength. For applications that require high signal strength, it is necessary to increase the recombination radiation of carriers instead of nonradiative recombination. However, for some applications that do not require high optical power, on the premise of ensuring a certain SNR, we can appropriately increase the nonradiative recombination ratio to reduce the recombination life of carriers, which is conducive to improving the modulation bandwidth of devices to achieve higher transmission rate.

6. Conclusion

To conclude, we present a comprehensive review on the state-of-the-art for improving the modulation bandwidth of GaN-based LEDs and WLEDs for high-speed visible light communication. Epitaxial approaches including c-polar facet epitaxial optimization, epitaxial growth on non/semipolar facet, and chip scheme such as micro-LEDs, nano-LEDs, RC-LEDs, plasmon, and meta-cavity LEDs have been reviewed and the corresponding challenges have been discussed. Approaches to tackle the slow

Stokes transfer and long carrier life for conventional phosphors including new CCMs and new energy transfer routes, such as plasmon-mediated transfer and NRET, have been introduced. Lastly, we have presented a brief analysis of the modulation depth and power–current linearity on the modulation width. This review should advance the research and development of GaN-based LEDs and WLEDs, toward a large modulation bandwidth and high-speed visible light communication.

Acknowledgments

National Key Research and Development Program of China (2018YFB0406702); Fundamental Research Funds for the Central Universities of Central South University (2018zzts147).

Conflict of Interest

The authors declare no conflict of interest.

Keywords

GaN, light-emitting diodes, modulation bandwidth, visible light communication

Received: April 21, 2021

Revised: July 10, 2021

Published online: September 23, 2021

- [1] H. Haas, L. Yin, Y. Wang, C. Chen, *J. Lightwave Technol.* **2016**, *34*, 1533.
- [2] Y. Tanaka, T. Komine, S. Haruyama, M. Nakagawa, in *12th IEEE Int. Symp. Personal, Indoor and Mobile Radio Communications*, IEEE, Piscataway, NJ **2001**.
- [3] S. Rajbhandari, J. J. D. McKendry, J. Herrnsdorf, H. Chun, G. Faulkner, H. Haas, I. M. Watson, D. O'Brien, M. D. Dawson, *Semicond. Sci. Technol.* **2017**, *32*, 023001.
- [4] J. Shi, K. Chi, J. Wun, J. E. Bowers, Y. Shih, J. Sheu, *IEEE Elect. Device L.* **2016**, *37*, 894.
- [5] K. Rajabi, J. Wang, J. Jin, Y. Xing, L. Wang, Y. Han, C. Sun, Z. Hao, Y. Luo, K. Qian, C. Chen, M. Wu, *Opt. Express* **2018**, *26*, 24985.
- [6] S. Zhu, S. Lin, J. Li, Z. Yu, H. Cao, C. Yang, J. Li, L. Zhao, *Appl. Phys. Lett.* **2017**, *111*, 171105.
- [7] H. Lan, I. Tseng, H. Kao, Y. Lin, G. Lin, C. Wu, *IEEE J. Quantum Elect.* **2018**, *54*, 3300106.
- [8] H. Lu, T. Yu, C. Jia, Y. Zhang, J. Wang, G. Zhang, *IEEE Photon. Tech. L.* **2016**, *28*, 1038.
- [9] C. Du, X. Huang, C. Jiang, X. Pu, Z. Zhao, L. Jing, W. Hu, Z. Wang, *Sci. Rep.* **2016**, *6*, 37132.
- [10] T. Wang, *Semicond. Sci. Technol.* **2016**, *31*, 093003.
- [11] R. P. Green, J. J. D. McKendry, D. Massoubre, E. Gu, M. D. Dawson, A. E. Kelly, *Appl. Phys. Lett.* **2013**, *102*, 091103.
- [12] M. Haemmer, B. Roycroft, M. Akhter, D. V. Dinh, Z. Quan, J. Zhao, P. J. Parbrook, B. Corbett, *IEEE Photon. Technol. Lett.* **2018**, *30*, 439.
- [13] A. Rashidi, M. Monavarian, A. Aragon, A. Rishinaramangalam, D. Feezell, *IEEE Electron. Device Lett.* **2018**, *39*, 520.
- [14] S. Huang Chen, Y. Huang, Y. Chang, Y. Lin, F. Liou, Y. Hsu, J. Song, J. Choi, C. Chow, C. Lin, R. Horng, Z. Chen, J. Han, T. Wu, H. Kuo, *ACS Photonics* **2020**, *7*, 2228.
- [15] S. H. Chen, Y. Huang, K. J. Singh, Y. Hsu, F. Liou, J. Song, J. Choi, P. Lee, C. Lin, Z. Chen, J. Han, T. Wu, H. Kuo, *Photonics Res.* **2020**, *8*, 630.
- [16] X. Zhou, P. Tian, C. Sher, J. Wu, H. Liu, R. Liu, H. Kuo, *Prog. Quant. Electron.* **2020**, *71*, 100263.
- [17] J. J. D. McKendry, R. P. Green, A. E. Kelly, Z. Gong, B. Guilhabert, D. Massoubre, E. Gu, M. D. Dawson, *IEEE Photon. Technol. Lett.* **2010**, *22*, 1346.
- [18] R. X. G. Ferreira, E. Xie, J. J. D. McKendry, S. Rajbhandari, H. Chun, G. Faulkner, S. Watson, A. E. Kelly, E. Gu, R. V. Penty, I. H. White, D. C. O'Brien, M. D. Dawson, *IEEE Photon. Technol. Lett.* **2016**, *28*, 2023.
- [19] Z. Sun, D. Teng, L. Liu, X. Huang, X. Zhang, K. Sun, Y. Wang, N. Chi, G. Wang, *IEEE Photon. J.* **2016**, *8*, 7904308.
- [20] H. Huang, H. Wu, C. Huang, Z. Chen, C. Wang, Z. Yang, H. Wang, *Phys. Status Solidi A* **2018**, *215*, 1800484.
- [21] J. J. D. McKendry, D. Massoubre, S. Zhang, B. R. Rae, R. P. Green, E. Gu, R. K. Henderson, A. E. Kelly, M. D. Dawson, *J. Lightwave Technol.* **2012**, *30*, 61.
- [22] S. Zhang, S. Watson, J. J. D. McKendry, D. Massoubre, A. Cogman, E. Gu, R. K. Henderson, A. E. Kelly, M. D. Dawson, *IEEE Photon. Conf.* **2012**.
- [23] T. K. Kim, M. U. Cho, J. B. So, J. M. Lee, S. K. Oh, Y. Cha, T. Jang, J. Cho, J. S. Kwak, *Jpn. J. Appl. Phys.* **2019**, *58*, SCCC12.
- [24] M. S. Islam, R. X. Ferreira, X. He, E. Xie, S. Videv, S. Viola, S. Watson, N. Bamiedakis, R. V. Penty, I. H. White, A. E. Kelly, E. Gu, H. Haas, M. D. Dawson, *Photonics Res.* **2017**, *5*, 35.
- [25] Y. Yin, W. Lan, T. Lin, C. Wang, M. Feng, J. Huang, *J. Lightwave Technol.* **2017**, *35*, 258.
- [26] T. Lin, Y. Chen, Y. Yin, Z. You, H. Kao, C. Huang, Y. Lin, C. Tsai, G. Lin, J. Huang, *IEEE Trans. Electron Devices* **2018**, *65*, 4375.
- [27] M. Nami, A. Rashidi, M. Monavarian, S. Mishkat-Ul-Masabih, A. K. Rishinaramangalam, S. R. J. Brueck, D. Feezell, *ACS Photonics* **2019**, *6*, 1618.
- [28] L. Wang, Z. Liu, Z. Li, Y. Zhang, H. Li, X. Yi, J. Wang, G. Wang, J. Li, *Nanoscale* **2017**, *9*, 7021.
- [29] E. F. Schubert, N. E. Hunt, M. Micovic, R. J. Malik, D. L. Sivco, A. Y. Cho, G. J. Zydzik, *Science* **1994**, *265*, 943.
- [30] A. Shaw, J. F. Donegan, J. G. Lunney, L. Bradley, *Proc. SPIE* **2003**, *4876*, 184.
- [31] M. Akhter, P. Maaskant, B. Roycroft, B. Corbett, P. de Mierry, B. Beaumont, K. Panzer, *Electron. Lett.* **2002**, *38*, 1457.
- [32] C. Tsai, Z. Xu, *IEEE Photon. Technol. Lett.* **2013**, *25*, 1793.
- [33] T. Lu, S. Chen, T. Wu, P. Tu, C. Chen, C. Chen, Z. Li, H. Kuo, S. Wang, *Appl. Phys. Lett.* **2010**, *97*, 071114.
- [34] W. Liu, X. Hu, L. Ying, J. Zhang, B. Zhang, *Appl. Phys. Lett.* **2014**, *104*, 251116.
- [35] W. Cai, J. Yuan, S. Ni, Z. Shi, W. Zhou, Y. Liu, Y. Wang, H. Amano, *Appl. Phys. Express* **2019**, *12*, 032004.
- [36] K. Okamoto, I. Niki, A. Scherer, Y. Narukawa, T. Mukai, Y. Kawakami, *Appl. Phys. Lett.* **2005**, *87*, 071102.
- [37] S. Zhu, Z. Yu, L. Zhao, J. Wang, J. Li, *Opt. Express* **2015**, *23*, 13752.
- [38] C. Yang, A. A. Bettiol, Y. Shi, M. Bosman, H. R. Tan, W. P. Goh, J. H. Teng, E. J. Teo, *Adv. Opt. Mater.* **2015**, *3*, 1703.
- [39] L. Ferrari, J. S. T. Smalley, H. Qian, A. Tanaka, D. Lu, S. Dayeh, Y. Fainman, Z. Liu, *ACS Photonics* **2018**, *5*, 3557.
- [40] S. Gong, J. Kim, Y. Ko, C. Rodriguez, J. Shin, Y. Lee, L. S. Dang, X. Zhang, Y. Cho, *Proc. Natl. Acad. Sci. USA* **2015**, *112*, 5280.
- [41] W. Zhou, M. Dridi, J. Y. Suh, C. H. Kim, D. T. Co, M. R. Wasielewski, G. C. Schatz, T. W. Odom, *Nat. Nanotechnol.* **2013**, *8*, 506.
- [42] K. Shen, C. Hsieh, Y. Cheng, D. P. Tsai, *Nano Energy* **2018**, *45*, 353.
- [43] H. V. Demir, S. Nizamoglu, T. Erdem, E. Mutlugun, N. Gaponik, A. Eychmuller, *Nano Today* **2011**, *6*, 632.

- [44] Z. Tian, P. Tian, X. Zhou, G. Zhou, S. Mei, W. Zhang, X. Zhang, D. Li, D. Zhou, R. Guo, S. Qu, A. L. Rogach, *Nanoscale* **2019**, *11*, 3489.
- [45] Z. Zhou, P. Tian, X. Liu, S. Mei, D. Zhou, D. Li, P. Jing, W. Zhang, R. Guo, S. Qu, A. L. Rogach, *Adv. Sci.* **2018**, *5*, 1800369.
- [46] X. Zhou, P. Tian, C. W. Sher, J. Wu, H. Liu, R. Liu, H. C. Kuo, *Prog. Quant. Electron.* **2020**, *71*, 100263.
- [47] H. Cao, S. Lin, Z. Ma, X. Li, J. Li, L. Zhao, *IEEE Electron. Device Lett.* **2019**, *40*, 267.
- [48] H. Chun, P. Manousiadis, S. Rajbhandari, D. A. Vithanage, G. Faulkner, D. Tsonev, J. J. D. McKendry, S. Videv, E. Xie, E. Gu, M. D. Dawson, H. Haas, G. A. Turnbull, I. D. W. Samuel, D. C. O'Brien, *IEEE Photon. Technol. Lett.* **2014**, *26*, 2035.
- [49] Z. Zhuang, X. Guo, B. Liu, F. Hu, Y. Li, T. Tao, J. Dai, T. Zhi, Z. Xie, P. Chen, D. Chen, H. Ge, X. Wang, M. Xiao, Y. Shi, Y. Zheng, R. Zhang, *Adv. Funct. Mater.* **2016**, *26*, 36.
- [50] M. Khoury, H. Li, P. Li, Y. C. Chow, B. Bonef, H. Zhang, M. S. Wong, S. Pinna, J. Song, J. Choi, J. S. Speck, S. Nakamura, S. P. DenBaars, *Nano Energy* **2020**, *67*, 104236.
- [51] R. Wan, X. Gao, L. Wang, S. Zhang, X. Chen, Z. Liu, X. Yi, J. Wang, J. Li, W. Zhu, J. Li, *Photonics Res.* **2020**, *8*, 1110.
- [52] P. Tian, Z. Wu, X. Liu, Z. Fang, S. Zhang, X. Zhou, K. Liu, M. Liu, S. Chen, C. Lee, C. Cong, L. Hu, Z. Qiu, L. Zheng, R. Liu, *Appl. Phys. Express* **2018**, *11*, 044101.
- [53] S. Zhu, X. Chen, X. Liu, G. Zhang, P. Tian, *Prog. Quant. Electron.* **2020**, *73*, 100274.
- [54] S. Mei, X. Liu, W. Zhang, R. Liu, L. Zheng, R. Guo, P. Tian, *ACS Appl. Mater. Interfaces* **2018**, *10*, 5641.
- [55] D. Xue, C. Ruan, Y. Zhang, H. Chen, X. Chen, C. Wu, C. Zheng, H. Chen, W. W. Yu, *Nanotechnology* **2018**, *29*, 455708.
- [56] C. Ruan, Y. Zhang, M. Lu, C. Ji, C. Sun, X. Chen, H. Chen, V. L. Colvin, W. W. Yu, *Nanomaterials* **2016**, *6*, 13.
- [57] Z. Wang, Z. Wang, B. Lin, X. Hu, Y. Wei, C. Zhang, B. An, C. Wang, W. Lin, *ACS Appl. Mater. Interfaces* **2017**, *9*, 35253.
- [58] X. Xiao, H. Tang, T. Zhang, W. Chen, W. Chen, D. Wu, R. Wang, K. Wang, *Opt. Express* **2016**, *24*, 21577.



Rongqiao Wan received his Ph.D. from Central South University of China in 2021. Currently, he works in Guilin University of Electronic Technology. His current research interests focus on III-nitride optoelectronic device.



Liancheng Wang received his Ph.D. from Institute of Semiconductors, Chinese Academy of Sciences. Then he worked as a research fellow in School of Electrical and Electronic Engineering, Nanyang Technological University, followed by Engineering Product Department, Singapore University of Technology and Design (SUTD) and Nitrides Center at the University of Sheffield, UK. Currently, he is a full professor at College of Mechanical and Electrical Engineering, Central South University, China. With over 110 peer-reviewed papers published, Dr. Wang's research interests include III-nitride semiconductor material, device, and microsystem.



Jinpeng Huang studied in School of Mechanical and Electrical Engineering, Central South University. His research focuses on the third-generation semiconductor display devices.



Xiaoyan Yi, Ph.D., is a professor, and the deputy director and chief engineer of Semiconductor Lighting R&D Center, Institute of Semiconductors, Chinese Academy of Sciences. Her primary research interest includes the field of nitride materials, devices design, device processing and fabrication, and device characterization. She has made pioneering contributions in the development of solid-state lighting in China and participated in several national projects of nitrides field about high-power LED structure design and key technology research.



Hao-Chung Kuo received his Ph.D. degree from the ECE, University of Illinois at Urbana Champaign, in 1999. He was in the Technical Program Committee for several major technical conferences for the IEEE, the OSA, and the SPIE, which include IEEE/OSA CLEO (2009–present), SPIE Photonics West (2009–present), and others. He serves as a panel member for Taiwan MOST (Photonic Program). He was the guest editor of the IEEE JSTQE (2009) and was an associate editor of the OSA/IEEE Journal of lightwave technology (2008–2013) and associate editor of the OSA Photonics Research (2019–present).



Jinmin Li received his Ph.D. degree in optics from Xi'an Institute of Optics and Precision Mechanics, Chinese Academy of Sciences, in 1991. His research interests focus on compound semiconductor single crystal materials and nitride materials epitaxy. He has made outstanding contributions to the research and development of optoelectronic devices, and optics for optical communications and solid-state lighting.